remote sensing

MDPI

Article

Study of Fast and Reliable Time Transfer Methods Using Low Earth Orbit Enhancement

Mingyue Liu [1,2,3], Rui Tu [1,2,3,4,*], Qiushi Chen [5], Qi Li [6], Junmei Chen [6], Pengfei Zhang [1,2,3] and Xiaochun Lu [1,2,3]

1 National Time Service Center, Chinese Academy of Sciences, Shu Yuan Road, Xi'an 710600, China
2 University of Chinese Academy of Sciences, Yu Quan Road, Beijing 100049, China
3 Key Laboratory of Lime Reference and Applications, Chinese Academy of Sciences, Shu Yuan Road, Xi'an 710600, China
4 College of Geodesy and Geomatics, Shandong University of Science and Technology, Qingdao 266590, China
5 College of Information and Navigation, Air Force Engineering University, East of Feng Gao Road, Xi'an 710077, China; chenqiushi@126.com
6 Qilu Aerospace Information Research Institute, No. 9 Kuang Yuan Road, Jinan 250100, China; liqi202929@aircas.ac.cn (Q.L.)
* Correspondence: turui-2004@126.com

Abstract: The Global Navigation Satellite System (GNSS) can be utilized for long-distance and high-precision time transmission. With the ongoing development of low Earth orbit (LEO) satellites and the rapidly changing geometric relationships between them, the convergence rate of ambiguity parameters in Precise Point Positioning (PPP) algorithms has increased, enabling fast and reliable time transfer. In this paper, GPS is used as an experimental case, the LEO satellite constellation is designed, and simulated LEO observation data are generated. Then, using the GPS observation data provided by IGS, a LEO-enhanced PPP model is established. The LEO-augmented PPP model is employed to facilitate faster and more reliable high-precision time transfer. The application of the LEO-augmented PPP model to time transfer is examined and discussed through experimental examples. These examples show multiple types of time transfer links, and the experimental outcomes are uniform. GPS + LEO is compared with exclusive GPS time transfer schemes. The clock offset of the time transfer link for the GPS + LEO scheme converges more swiftly, meaning that the time required for the clock offset to reach a stable level is the briefest. In this paper, standard deviation is employed to assess stability, and Allan deviation is utilized to assess frequency stability. The results show that the clock offset stability and frequency stability achieved by the GPS + LEO scheme are superior within the convergence time range. Controlled experiments with different numbers of satellites for LEO enhancement indicate that time transfer performance can be improved by increasing the number of satellites. As a result, augmenting GPS tracking data with LEO observations enhances the time transfer service compared to GPS alone.

Keywords: low Earth orbit satellite; precise point positioning; global navigation satellite system; time transfer

Citation: Liu, M.; Tu, R.; Chen, Q.; Li, Q.; Chen, J.; Zhang, P.; Lu, X. Study of Fast and Reliable Time Transfer Methods Using Low Earth Orbit Enhancement. *Remote Sens.* **2024**, *16*, 2044. https://doi.org/10.3390/rs16112044

Academic Editors: Kamil Krasuski and Damian Wierzbicki

Received: 29 April 2024
Revised: 4 June 2024
Accepted: 4 June 2024
Published: 6 June 2024

1. Introduction

The technology of time transfer has resolved the problem of synchronizing clocks between two locations. Currently, time transfer can be executed through a variety of methods, including fiber optics, broadcast radio signals, telephones, networks, and more. The Global Navigation Satellite System (GNSS) time transfer method, which employs radio signals for time transfer, offers extensive coverage, high accuracy, and ease of operation [1]. In recent years, GNSS time transfer based on Precise Point Positioning (PPP) solutions has experienced rapid development [2]. The PPP method combines pseudorange and carrier-phase observation data, with precision products, such as precise orbits and clock deviations, to achieve high-precision time transfer services [3]. Zhang et al., achieved PPP time transfer with an accuracy

of 0.1–0.2 ns and frequency stability of 1×10^{-15}–2×10^{-15} in half a day using International GNSS Service (IGS) precise satellite clock differential products [4]. However, attaining PPP time transfer accuracy at the sub-nanosecond level typically necessitates a substantial amount of convergence time, spanning several tens of minutes [5]. In practical applications of GNSS time transfer, the method's real-time reliability is affected by environmental interference on the receiving terminal when receiving satellite signals [6,7].

Numerous scholars have engaged in research aimed at enhancing the performance of PPP time transfer. Zhao et al. [8] proposed a method to enhance PPP time transfer stability by constraining receiver clock offset, resulting in a significant short-term stability improvement. Xu et al. [9] created a multi-frequency ionosphere elimination PPP time transfer model for the BeiDou Satellite Navigation System (BDS). The tri-frequency PPP time transfer achieved an accuracy of 0.61 ns and the dual-frequency accuracy was 0.75 ns, demonstrating the advantages and feasibility of BDS tri-frequency PPP in time transfer applications. Lv et al. [10] performed PPP time transfer by incorporating multi-GNSS observations and ambiguity fixing techniques. The results demonstrated that integrating multi-system observations into PPP time transfer reduced the standard deviation by 38.1% compared to the traditional GPS-only approach.

In addition to the aforementioned methods that enhance PPP time transfer performance through parameter constraints, multiple frequencies, and multi-system integration, the advent of low Earth orbit (LEO) satellites has introduced a novel avenue for performance enhancement. Since the 1990s, numerous organizations have launched constellations of low Earth orbit (LEO) communications satellites, with the LEO Iridium U.S. communications satellite constellation being the most prevalent example. [11]. Compared with GNSS satellites, LEO satellites offer an increased signal strength and a faster geometry change due to their lower orbital altitudes. This confers robust anti-spoofing and anti-jamming capabilities, ensuring normal continuous signal reception in signal-obscuring environments [6,12]. The ongoing evolution of LEO satellites has led to new advancements in Global Navigation Satellite Systems. Reid et al. [13,14] established the viability of developing integrated positioning, navigation, and timing (PNT) systems with LEO satellites by analyzing signal strength, propagation times, and the geometric dynamics between LEO satellites. This confirms that LEO-augmented GNSS systems are achievable. Ke et al. [15] formulated a PPP model for ionospheric removal using GPS and LEO satellites. They confirmed that GPS combined with LEO satellites allows for a shorter PPP convergence time than just processing sole GPS data. Ge et al. [16] created simulation software to simulate GNSS and LEO observations from ground stations. Their simulation outcomes indicated that LEO-augmented GNSS could reduce the PPP convergence time to 5 min. Su et al. [17] assessed the performance of BDS-3 enhanced by an LEO satellite constellation through data simulation, and the findings demonstrated that the PPP convergence time was decreased from approximately 30 min to 1 min. Zhao et al. [2] appraised the efficacy of the integrated LEO/GNSS PPP under adverse environmental conditions and executed comparative experiments with observational simulations, revealing that the convergence velocity and precision of both fixed and floating solutions derived from the LEO enhancement of GNSS were enhanced. Li et al. [18] developed three types of LEO constellations with 60,192 and 288 satellites and simulated the observation data with GNSS observations over the ground station. Concurrently, the LEO constellation was designed to transmit navigation signals at three frequencies: L1, L2 and L5. The results demonstrated that the introduction of LEO constellations can markedly enhance the performance of both single-system and multi-GNSS PPP AR. Li et al. [19] studied the feasibility of providing real-time PPP services with LEO-augmented GNSS. The results confirmed that LEO-augmented GNSS can accomplish spatial signal ranging with an error at the centimeter level.

Based on the aforementioned studies, the integration GNSS with LEO satellites can enhance the performance of PPP. However, a scarcity of studies have applied LEO enhancement to time transfer. Consequently, this study concentrates on the application of LEO-augmented GNSS to time transfer. This paper employs GPS data as a case study. By

designing a constellation of LEO satellites and simulating satellite observations, we conducted an analysis of the performance of GPS time transfer enhanced by LEO, incorporating actual GPS observation data.

2. Experimental Principles

2.1. LEO Constellation Design and Observation Simulation

To investigate the time transfer performance of the GNSS enhanced by LEO satellites, due to the lack of existing observation data of low orbit satellites, this study simulates the observation data of low orbit satellites. The simulation of observation data is the inverse process of positioning calculation [20]. The simulated observation data of low orbit used in this study are obtained by introducing various types of errors into the geometric distance between the satellites and the receivers. Since GNSS observations use GPS, for ease of interoperability, the simulated observation frequency for the LEO satellites is the same as that of GPS, 1575.42 MHz (L1) and 1227.60 MHz (L2). Before the simulation, fixed station coordinates, receiver clock bias, and zenith tropospheric delay are obtained through a static PPP solution in preparation for subsequent simulations.

First, the LEO satellite constellation is designed with simulated orbits and clock discrepancies. This study simulates 160 low Earth orbit satellites, with 70 distributed across six polar orbits and 90 across ten inclined orbits. The inclination of the polar orbits is 90°, while the inclination of the inclined orbits is 60° [21,22]. The low Earth orbit satellite group adopts a Walker constellation, which consists of multiple circular orbit satellites with the same orbital altitude, with the satellite orbital height being 1000 km. For the simulation of the low Earth orbit satellite orbits, the initial positions and initial velocities of each satellite are calculated based on the aforementioned LEO constellation parameters, and then, the orbital dynamics are integrated to obtain full-day orbit data. The orbits are then transformed from the geocentric inertial coordinate system to the Earth-centered, Earth-fixed coordinate system (ECEF), with the orbital data interval designed to be 30 s for interoperability with IGS products. The simulation of orbit errors is achieved by combining cosine trend terms, constant trend terms, and Gaussian noise. The clock bias of the low Earth orbit satellites is simulated using the GPS satellite clock biases provided by IGS. Without considering the system time bias between LEO and GPS, the clock bias of GPS satellites is randomly substituted for the low Earth orbit satellites. The errors published by IGS are calculated clock biases from the IF combination (a linear combination of L1/L2), and the simulated clock errors absorb the pseudorange hardware delays of dual-frequency ionosphere-free combination satellites. It should be noted that the simulation results for orbit and clock errors may not be absolutely accurate, so further consideration should be given to systematic and random errors after combining satellite orbits and satellite clock errors. To simplify the process, noise of different magnitudes is directly added to the orbital components and satellite clock errors.

Geometric distances are calculated using known receiver coordinates, satellite orbits, and satellite clock errors. Then, various error terms are calculated using error models. Specifically, the ionospheric delay is calculated using the projection function and total electron content from the global ionospheric maps published by the Center for Orbit Determination in Europe (CODE). For the simulation of tropospheric delay, the wet component of the troposphere delay is calculated using static PPP estimation and the GMF (Global Mapping Function) projection function, while the dry component of the troposphere delay is calculated using the Saastamonien empirical model and GMF projection function [11,23]. The initial measurement noise for code and phase is simulated as Gaussian noise with a standard deviation of 0.5 m and 3 mm, respectively, and is inversely correlated with elevation angle. Earth rotation errors, relativistic effects, and tides are corrected using existing corresponding models. Finally, all types of errors are added to the geometric distance between the satellite and ground station to obtain the final observed data at the ground station.

2.2. LEO-Augmented PPP Model

In this study, we utilized both GNSS observation data and simulated LEO satellite observation data. The GNSS observation data encompassed pseudorange observations as well as carrier-phase observations. The PPP observation equation is constructed as follows:

$$P_{f,R}^{G,S} = \rho_R^{G,S} + c{\cdot}\delta T_R - c{\cdot}\delta T^{G,S} + \tau_{ion,f,R}^{G,S} + \tau_{trop} + \tau_{delay\_P,f,R}^{G} - \tau_{delay\_P,f}^{G,S} + \varepsilon_{P,f,R}^{G,S} \quad (1)$$

$$\Phi_{f,R}^{G,S} = \rho_R^{G,S} + c{\cdot}\delta T_R - c{\cdot}\delta T^{G,S} + \lambda_f^{G,S}(N_{f,R}^{G,S} + \tau_{delay\_\Phi,f,R}^{G} - \tau_{delay\_\Phi,f}^{G,S}) - \tau_{ion,f,R}^{G,S} + \tau_{trop} + \varepsilon_{\Phi,f,R}^{G,S} \quad (2)$$

where the superscript G indicates the GNSS system type; the superscript S indicates a specific satellite; the subscript f indicates the carrier frequency of the satellite signal; the subscript R indicates the receiver; $P_{f,R}^{G,S}$ is the pseudorange observation; $\rho_R^{G,S}$ is the geometric distance between the station and the satellite; c is the speed of light under vacuum conditions; δT_R is the receiver clock offset, which refers to the time deviation between the system time and the receiver clock; $\delta T^{G,S}$ is the satellite clock offset; $\tau_{ion,f,R}^{G,S}$ is the ionospheric delay at the f carrier frequency; τ_{trop} is the tropospheric delay; $\tau_{delay\_P,f,R}^{G}$ is the hardware delay related to the receiver code, $\tau_{delay\_P,f}^{G,S}$ is the code hardware delay on the satellite side, with the code calibration delay in meters; $\varepsilon_{P,f,R}^{G,S}$ is the pseudo-distance observation noise; $\Phi_{f,R}^{G,S}$ is the carrier-phase observation; $\lambda_f^{G,S}$ is the wavelength of the satellite carrier signal; $N_{f,R}^{G,S}$ is integer ambiguity; $\tau_{delay\_\Phi,f,R}^{G}$ is the hardware delay for the receiver phase, $\tau_{delay\_\Phi,f}^{G,S}$ is the hardware delay for the phase on the satellite end, with phase calibration delays in cycles; and $\varepsilon_{\Phi,f,R}^{G,S}$ is the carrier-phase observation noise.

In this study, to eliminate the first-order ionospheric delay of the pseudorange and carrier-phase observables, the ionosphere-free (*IF*) PPP model was employed as follows:

$$P_{IF,R}^{G,S} = \frac{(f_1^{G,S})^2 P_{1,R}^{G,S} - (f_2^{G,S})^2 P_{2,R}^{G,S}}{(f_1^{G,S})^2 - (f_2^{G,S})^2} \quad (3)$$

$$\Phi_{IF,R}^{G,S} = \frac{(f_1^{G,S})^2 \Phi_{1,R}^{G,S} - (f_2^{G,S})^2 \Phi_{2,R}^{G,S}}{(f_1^{G,S})^2 - (f_2^{G,S})^2} \quad (4)$$

where $f_1^{G,S}$ and $f_2^{G,S}$ are the frequencies of different carrier signals.

Therefore, the *IF*-PPP model observation equation is as follows:

$$P_{IF,R}^{G,S} = \rho_R^{G,S} + c{\cdot}\delta T_R - c{\cdot}\delta T^{G,S} + \tau_{trop} + \tau_{delay\_P,IF,R}^{G} - \tau_{delay\_P,IF}^{G,S} + \varepsilon_{P,IF,R}^{G,S} \quad (5)$$

$$\Phi_{IF,R}^{G,S} = \rho_R^{G,S} + c{\cdot}\delta T_R - c{\cdot}\delta T^{G,S} + \lambda_{IF}^{G,S}(N_{IF,R}^{G,S} + \tau_{delay\_\Phi,IF,R}^{G} - \tau_{delay\_\Phi,IF}^{G,S}) + \tau_{trop} + \varepsilon_{\Phi,IF,R}^{G,S} \quad (6)$$

The ionosphere-free combination code pseudorange hardware delay at the satellite end and the receiver end is absorbed by the ambiguity parameters. So, Formulas (5) and (6) are rewritten as Formulas (7) and (8), respectively.

$$P_{IF,R}^{G,S} = \rho_R^{G,S} + c{\cdot}\overline{\delta} T_R^G + \tau_{trop} + \varepsilon_{P,IF,R}^{G,S} \quad (7)$$

$$\Phi_{IF,R}^{G,S} = \rho_R^{G,S} + c{\cdot}\overline{\delta} T_R^G + \lambda_{IF}^{G,S}\overline{N}_{IF,R}^{G,S} + \tau_{trop} + \varepsilon_{\Phi,IF,R}^{G,S} \quad (8)$$

The reparameterized receiver clock error and ambiguity are shown in Formula (9):

$$\begin{cases} c\cdot\overline{\delta}T_R^G = c\cdot\delta T_R + \tau_{delay\_P,IF,R}^G \\ \overline{N}_{IF,R}^{G,S} = N_{IF,R}^{G,S} + \tau_{UPD,IF,R}^G - \tau_{UPD,IF}^{G,S} \\ \tau_{UPD,IF,R}^G = \tau_{delay\_\Phi,IF,R}^G - \tau_{delay\_P,IF,R}^G/\lambda_{IF}^{G,S} \\ \tau_{UPD,IF}^{G,S} = \tau_{delay\_\Phi,IF}^{G,S} - \tau_{delay\_P,IF}^{G,S}/\lambda_{IF}^{G,S} \end{cases} \tag{9}$$

where $\tau_{UPD,IF,R}^G$ is the uncalibrated phase delay at the receiver end; $\tau_{UPD,IF}^{G,S}$ is the uncalibrated phase delay at the satellite end; and $\overline{N}_{IF,R}^{G,S}$ is the *IF* combined ambiguity parameter, which contains the hardware delay deviation at the satellite and receiver ends.

By combining the simulated observational data from the LEO satellites, the PPP model for LEO enhancement was constructed as follows:

$$\begin{cases} P_{IF,R}^{G,S} = \rho_R^{G,S} + c\cdot\overline{\delta}T_R^G + \tau_{trop} + \varepsilon_{P,IF,R}^{G,S} \\ \Phi_{IF,R}^{G,S} = \rho_R^{G,S} + c\cdot\overline{\delta}T_R^G + \lambda_{IF}^{G,S}\overline{N}_{IF,R}^{G,S} + \tau_{trop} + \varepsilon_{\Phi,IF,R}^{G,S} \\ P_{IF,R}^{L,S} = \rho_R^{L,S} + c\cdot\overline{\delta}T_R^L + \tau_{trop} + \varepsilon_{P,IF,R}^{L,S} \\ \Phi_{IF,R}^{L,S} = \rho_R^{L,S} + c\cdot\overline{\delta}T_R^L + \lambda_{IF}^{L,S}\overline{N}_{IF,R}^{L,S} + \tau_{trop} + \varepsilon_{\Phi,IF,R}^{L,S} \end{cases} \tag{10}$$

Among them, the *L* superscript represents the LEO satellite.

3. Experimental Method

3.1. Data Source

To investigate the impact of the GNSS PPP model with LEO-augmented GNSS time transfer performance, we used the GPS observation data provided by the IGS for day 1 in 2022 and the related precise products. A cohort of 13 stations was curated based on equipment type and geographic location. The station coordinates were fixed during PPP solving, and the station information is shown in Table 1 below.

Table 1. List of selected measurement station information.

Station	Latitude (°)	Longitude (°)	Elevation (m)	Clock Type
areg	−16.5	−71.5	2489.7	EXTERNAL RUBIDIUM
mcil	24.3	154.0	36.1	EXTERNAL RUBIDIUM
bor1	52.3	17.1	125.3	EXTERNAL H-MASER
gold	35.4	−116.9	987.1	EXTERNAL H-MASER
ons1	57.4	11.9	44.9	EXTERNAL H-MASER
pie1	34.3	−108.1	2348.1	EXTERNAL H-MASER
usud	36.1	138.4	1509.0	EXTERNAL H-MASER
ohi2	−63.3	−57.9	33.1	EXTERNAL H-MASER
dlf1	52.0	4.4	76.3	EXTERNAL CESIUM
harb	−25.9	27.7	1558.5	EXTERNAL CESIUM
kiru	67.9	21.0	391.3	EXTERNAL CESIUM
sydn	−33.8	151.2	86.0	EXTERNAL CESIUM
syog	−69.0	39.6	50.1	EXTERNAL CESIUM

Utilizing the aforementioned stations, ten time transfer links were established. The time transfer link information is shown in Table 2, and the spatial distribution of the ten time transfer links is illustrated in Figure 1.

With regard to the LEO satellite observation data, the ground station of the MGEX observation network was used to simulate the LEO satellite ground observation data based on the above LEO satellite observation simulation method. The daily average number of visible satellites in the LEO constellation on the first day of 2022 is shown in Figure 2. The relevant data used in the study are presented in Table 3.

Table 2. Time transfer link information.

Time Transfer Link	Distance (km)	Location	Clock Type
areg-mcil	11,858.8	Low latitude	Rubidium clocks
gold-pie1	811.0	Mid latitude	Hydrogen clock
pie1-ons1	7814.0	Mid latitude	Hydrogen clock
ons1-bor1	658.2	Mid latitude	Hydrogen clock
bor1-usud	8031.1	Mid latitude	Hydrogen clock
kiru-dif1	1973.8	Mid-to-high latitude	Cesium clock
dlf1-harb	8205.9	Mid–low latitude	Cesium clock
harb-sydn	9763.0	Mid–low latitude	Cesium clock
kiru-syog	11,842.8	High latitude	Cesium clock
ohi2-syog	3908.6	High latitude	Hydrogen–Cesium clock

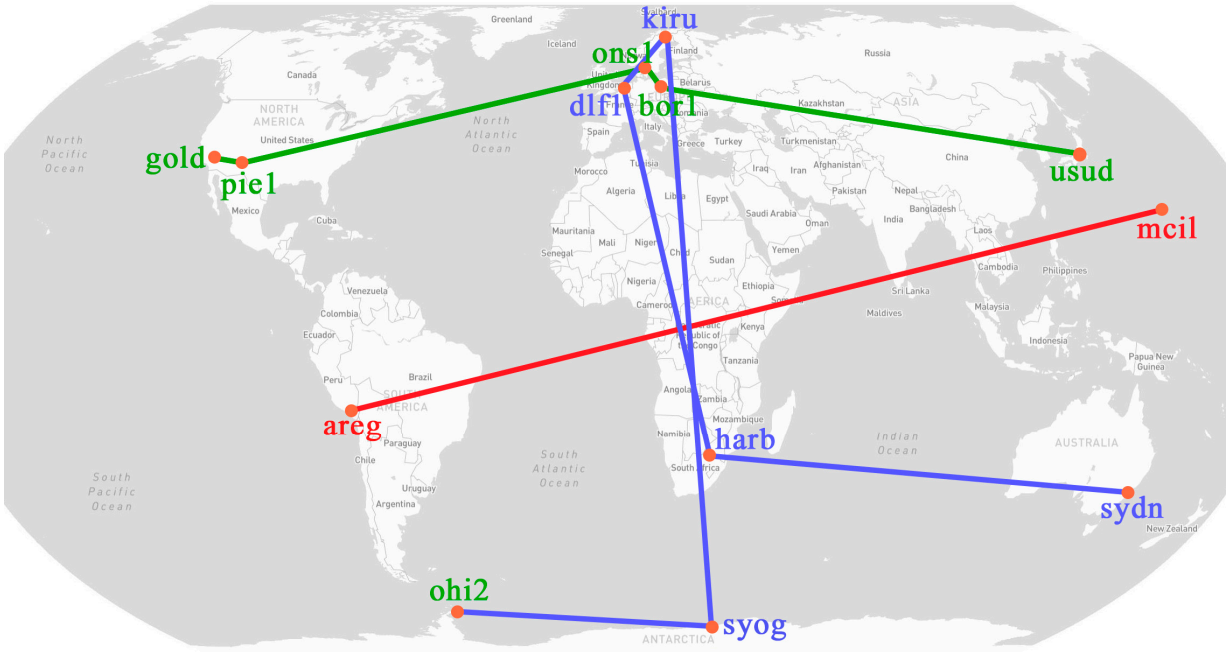

Figure 1. Global distribution of stations and time transfer links.

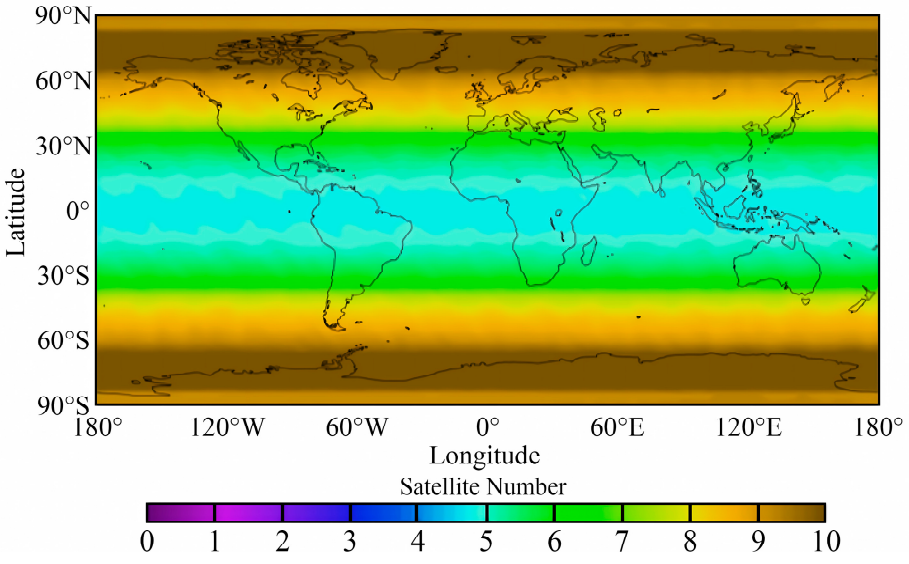

Figure 2. Average number of daily visible satellites of the LEO constellation on the first day of 2022.

Table 3. Data introduction.

Type	Descriptions
Data sources	GPS, LEO
Data characteristics	GPS is measured data LEO is analogue data
Type of observation	Pseudorange and phase observations
Frequency	L1, L2
Types of LEO constellations and number of satellites	70 satellites in polar orbit and 90 satellites in inclined orbit
LEO satellite altitude	1000 km

3.2. Experimental Solution

To analyze the effects of LEO enhancement on GPS time transfer performance, a sole GPS time transfer experiment was carried out. We used the following two experimental schemes for the comparative analysis of time transfer performance:

Solution A: Time transfer using a sole GPS system.
Solution B: Time transfer using GPS combined with LEO satellites.

To verify the applicability of LEO-augmented GPS time transfer at different latitudes and its performance with different numbers of satellites, we designed time transfer links and simulated different numbers of satellites.

4. Example Analysis

4.1. Analysis of LEO-Augmented GPS Time Transfer Convergence Performance

Three representative stations, namely areg, harb, and ons1, were selected to analyze the receiver clock offset calculated by LEO-augmented PPP. The three stations—areg, harb, and ons1—used rubidium, cesium, and hydrogen, respectively, as their clock frequencies. The first 30 min receiver clock offsets of the three stations are shown in Figure 3a–c, and the first-order difference results of the clock offsets are shown in Figure 4a–c. In the calculation, the three stations involved an average of eight low-orbit satellites. According to the clock offset variation diagram of the three stations, receiver clock offsets converge faster under LEO enhancement than under the sole GPS. To quantify the convergence time, by calculating the first-order difference of the receiver clock offset, the mean and standard deviation were calculated using the converged first-order difference data, and the convergence confidence interval was obtained by adding and subtracting the mean from two times the standard deviation. The convergence criterion was that the first-order difference result of the receiver clock offset should be within the range of the convergence confidence interval for 10 min. The red lines in Figure 4a–c represent the boundaries of the convergence confidence interval. The results of the statistical convergence time calculation are presented in Table 4 and Figure 5. According to the statistics, the convergence period was significantly shorter compared to processing sole GPS data and moreover significantly different at the three stations. The convergence speed increased the most (65.0%) at station harb, with its cesium clock; second-most (50.0%) at station ons1, with its hydrogen clock; and least (18.8%) at station areg, with its rubidium clock.

Table 4. Receiver clock offset convergence time improvement (min).

Station	GPS	GPS + LEO	Percentage of Improvement
areg	8	6.5	18.8%
harb	10	3.5	65.0%
ons1	11	5.5	50.0%

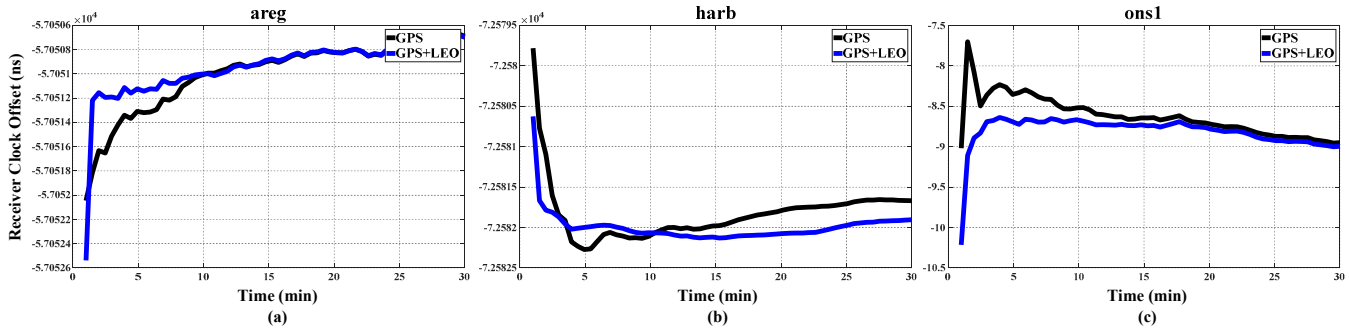

Figure 3. Receiver clock offset time series of stations (black denotes GPS alone; blue, GPS + LEOs.

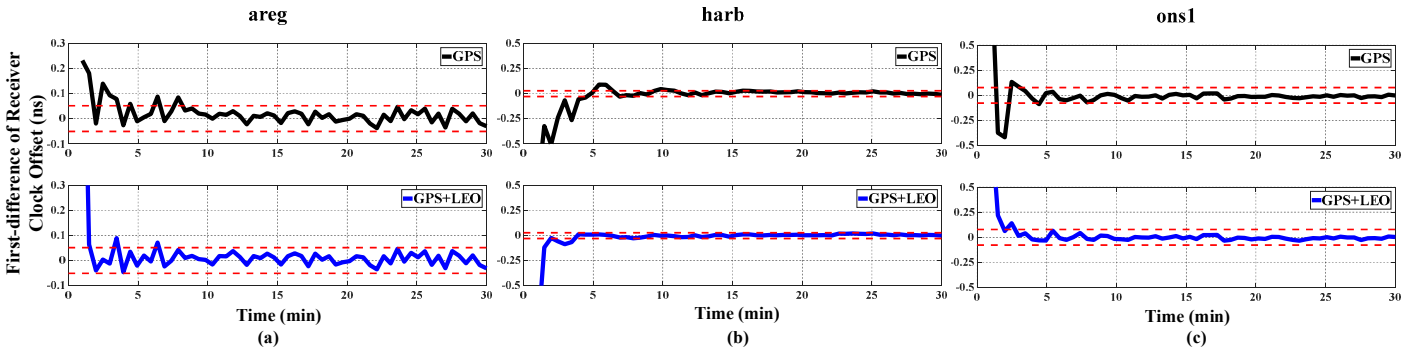

Figure 4. The first-order difference of the receiver clock offset time series of the stations (black denotes GPS alone; blue, GPS + LEOs). (**a**) The first-order difference results of the clock offset sequence for the areg station, (**b**) The first-order difference results of the clock offset sequence for the harb station, (**c**) The first-order difference results of the clock offset sequence for the ons1 station.

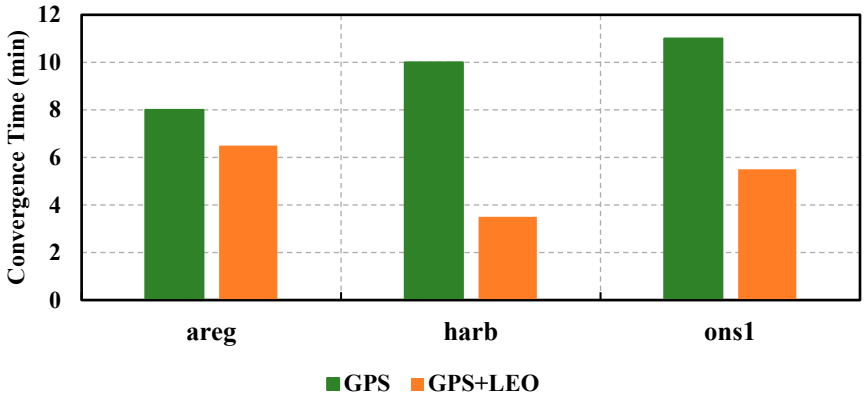

Figure 5. Receiver clock offset convergence time.

In light of the aforementioned conclusions, it can be posited that the receiver clock offset obtained by LEO-augmented PPP can effectively enhance convergence speed.

The clock offset of a time transfer link calculated for the established 10 links are shown in Figure 5. The time transfer link clock offset had the same performance as the receiver clock offset. The time transfer link achieved using LEO-augmented PPP exhibited a faster performance compared to that attained by the GPS system (Figure 6). Concurrently, the 10 links had different latitude distributions, baseline lengths, and clock sources. Although the different time transfer links had different characteristics, they exhibited similar performances. A first-order differential calculation was applied to the clock offset sequence of the time transfer link, and the convergence confidence interval

was determined. The results are presented in Figure 7. The first-order difference of the clock offset clearly showed faster convergence after LEO enhancement. The results of the convergence time calculations are presented in Table 5 and Figure 8.

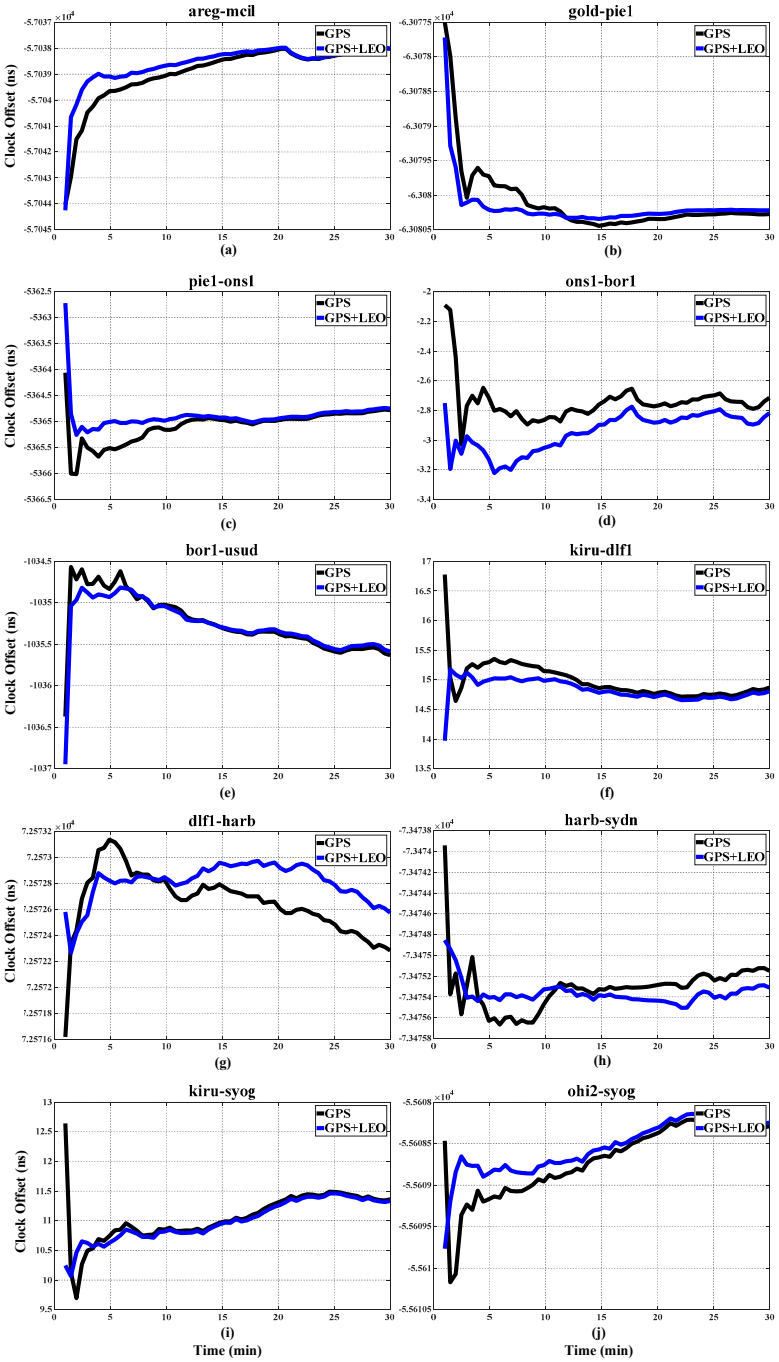

Figure 6. Time transfer link clock offset time series (black denotes GPS alone; blue GPS + LEOs). (**a**) The clock offset sequence of the areg-mcil time transfer link, (**b**) The clock offset sequence of the gold-pie1 time transfer link, (**c**) The clock offset sequence of the pie1-ons1 time transfer link, (**d**) The clock offset sequence of the ons1-bor1 time transfer link, (**e**) The clock offset sequence of the bor1-usud time transfer link, (**f**) The clock offset sequence of the kiru-dlf1 time transfer link, (**g**) The clock offset sequence of the dlf1-harb time transfer link, (**h**) The clock offset sequence of the harb-sydn time transfer link, (**i**) The clock offset sequence of the kiru-syog time transfer link, (**j**) The clock offset sequence of the ohi2-syog time transfer link.

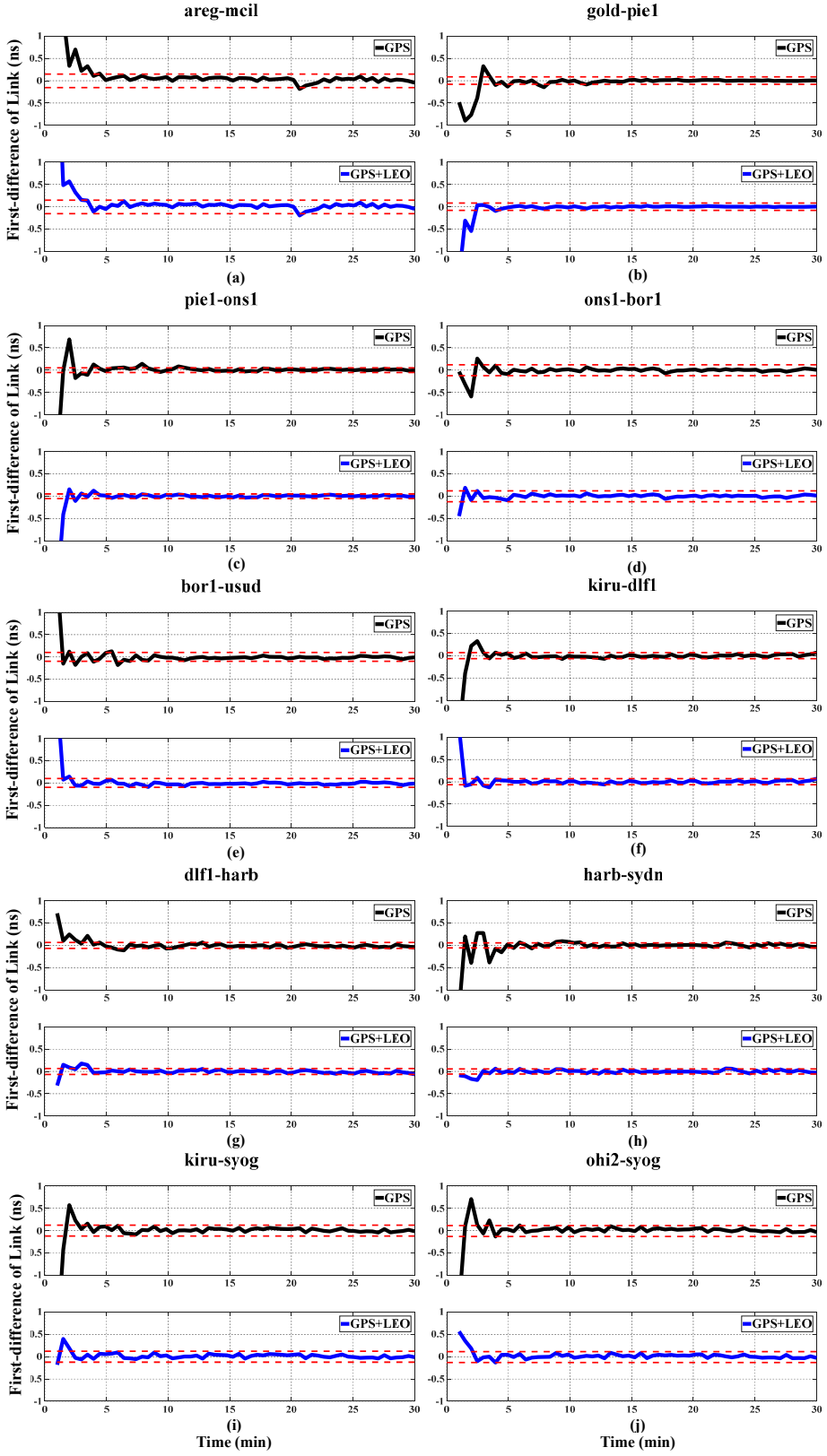

Figure 7. The first-order difference results of clock offsets time series in time transfer links (black denotes GPS alone; blue, GPS + LEOs). (**a**) The first-order difference results of the clock offset sequence for the areg-mcil time transfer link, (**b**) The first-order difference results of the clock offset

sequence for the gold-pie1 time transfer link, (**c**) The first-order difference results of the clock offset sequence for the pie1-ons1 time transfer link, (**d**) The first-order difference results of the clock offset sequence for the ons1-bor1 time transfer link, (**e**) The first-order difference results of the clock offset sequence for the bor1-usud time transfer link, (**f**) The first-order difference results of the clock offset sequence for the kiru-dlf1 time transfer link, (**g**) The first-order difference results of the clock offset sequence for the dlf1-harb time transfer link, (**h**) The first-order difference results of the clock offset sequence for the harb-sydn time transfer link, (**i**)The first-order difference results of the clock offset sequence for the kiru-syog time transfer link, (**j**) The first-order difference results of the clock offset sequence for the ohi2-syog time transfer link.

Table 5. Convergence time and percentage of improvement in time transfer links (min).

Links	GPS	GPS + LEO	Percentage of Improvement
areg-mcil	4.5	3	33.3%
gold-pie1	11.5	4	65.2%
pie1-ons1	11.5	4	65.2%
ons1-bor1	2.5	1.5	40.0%
bor1-usud	6	2	66.7%
kiru-dif1	13	3.5	73.1%
dlf1-harb	11	6	45.5%
harb-sydn	11	6	45.5%
kiru-syog	3.5	2	42.9%
ohi2-syog	6	4	33.3%

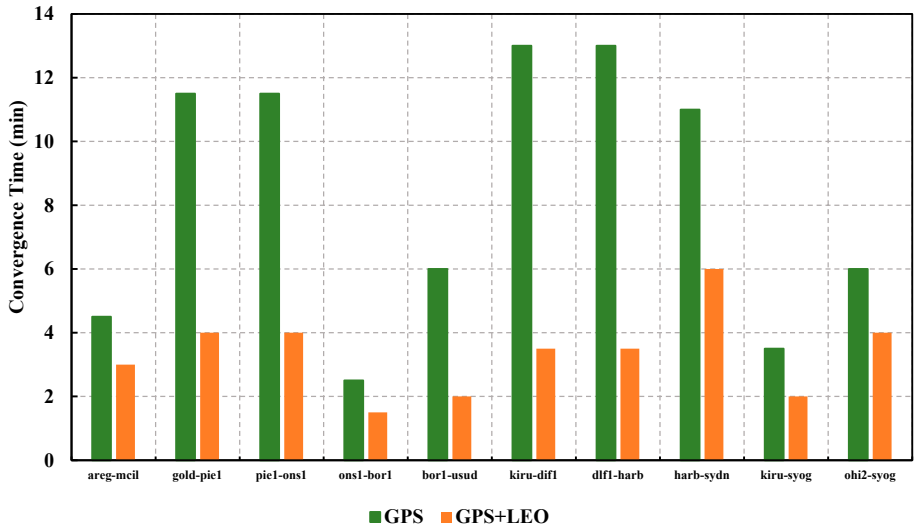

Figure 8. Time transfer link convergence time histogram.

The convergence speed of the time transfer link constructed by the rubidium clock link and the hydrogen–cesium hybrid clock group was the slowest. The performance of the rubidium clock link was consistent with the convergence speed of the receiver clock offset, which reflected the atomic clock performance. The kiru-dif1 link had the greatest increase in convergence speed among the cesium atomic clock links and was the link with the shortest baseline length among the four cesium atomic clock links. In the hydrogen atomic clock link, convergence time was consistently within four minutes. Therefore, LEO-augmented PPP exhibited different convergence speed improvements in time transfer links with different atomic clock and baseline lengths. There were no significant differences among time transfer links at different latitudes because the LEO constellations had wide latitude coverage. Thus, there was no significant latitude difference in the convergence speed of clock offsets in the LEO-augmented PPP time transfer links.

4.2. Stability Analysis of LEO-Augmented GPS Time Transfer

For the sustained and dependable application of GNSS time transfer, the reliability of the clock offset in the time transfer link is of paramount importance. Considering that LEO-augmented PPP can improve the convergence speed of time transfer links, the standard deviation of the clock offset obtained by the two methods in the convergence interval was examined. As evident from the results presented in Table 6 and Figure 9, the standard deviation of the clock offset for the LEO-augmented time transfer link exhibited a marked improvement within the convergence interval, when compared to that of GPS. Therefore, LEO-augmented PPP provides a higher stability in the initial convergence period of time transfer and can better ensure the stability and reliability of real-time fast convergence time transfer.

Table 6. Standard deviation of time transfer link clock offset in the convergence interval (ns).

Time Transfer Link	GPS	GPS + LEO	Percentage of Improvement
areg-mcil	0.491	0.358	27.1%
gold-pie1	0.228	0.047	79.3%
pie1-ons1	0.226	0.064	71.9%
ons1-bor1	0.302	0.133	55.9%
bor1-usud	0.202	0.159	21.2%
kiru-dlf1	0.158	0.081	48.8%
dlf1-harb	0.141	0.051	63.4%
harb-sydn	0.170	0.038	77.4%
kiru-syog	0.108	0.098	8.9%
ohi2-syog	0.176	0.096	45.6%

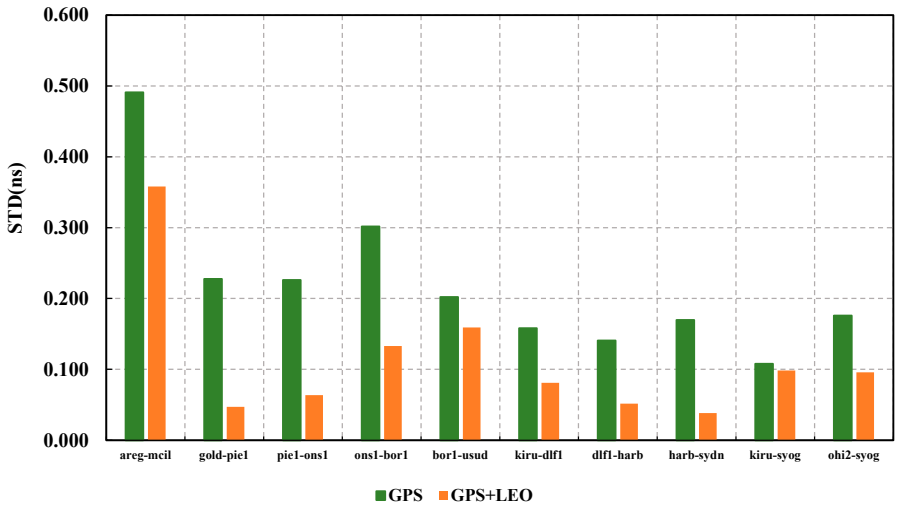

Figure 9. Histogram of standard deviation of time transfer link clock offsets in the convergence interval.

The time and frequency signals of the time transfer link are continuous. Time and frequency signals are not always fixed due to the influence of frequency source performance variation characteristics. However, this alteration has the same impact on the two data processing schemes [1], whether long-term or short-term. The Allan deviation is employed to assess the frequency stability of the time transfer clock offset sequence in the convergence time span. The Allan deviation results for each time transfer link are shown in Figure 10. The blue curve represents the Allan deviation obtained by the sole GPS time transfer scheme, and the orange curve represents the Allan deviation obtained by the GPS + LEO time transfer scheme. The Allan deviation obtained by the GPS + LEO time transfer scheme obviously shows a smaller variance. Thus, adding low-orbit satellites to the sole GPS data improves the frequency stability of the time transfer clock error sequence within

the convergence time range. The Allan deviation results for the 10 links were calculated and averaged. As depicted in Table 7, the frequency stability was improved after LEO enhancement over different sampling time intervals, with a minimum improvement of 25.7%. Consequently, within the time transfer convergence interval, LEO-enhanced PPP time transfer can effectively improve the frequency stability of the time transfer link's clock error sequence. The principal rationale is the fast geometry change in the low-orbit satellites, which allows for a faster and more stable estimation of the receivers' position and clock offset.

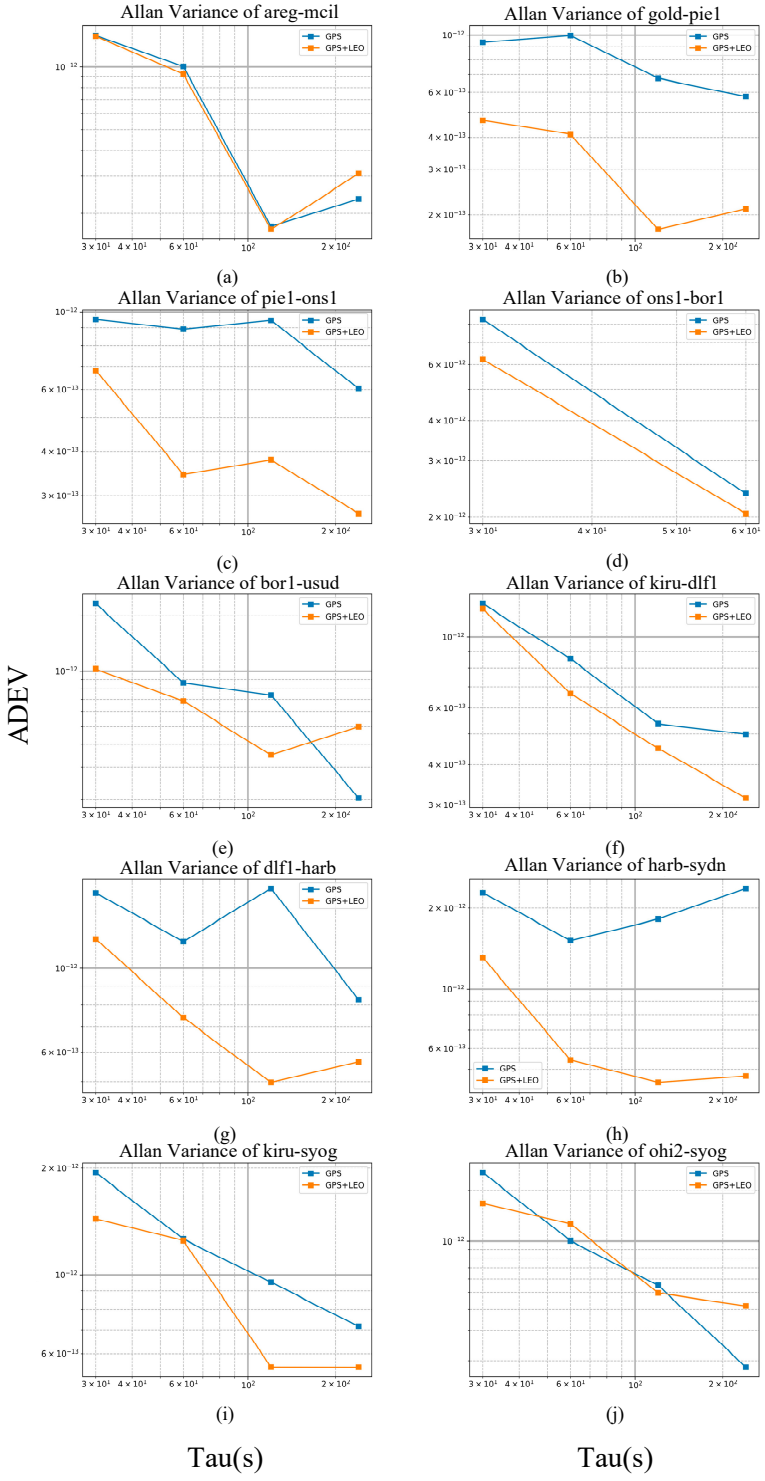

Figure 10. The Allan deviation results of the time transfer link in the convergence interval.

Table 7. Mean Allan deviation results.

Tau	GPS	GPS + LEO	Percentage of Improvement
30	2.35×10^{-12}	1.66×10^{-12}	29.2%
60	1.19×10^{-12}	8.87×10^{-13}	25.7%
120	8.92×10^{-13}	3.90×10^{-13}	56.2%
240	6.91×10^{-13}	4.01×10^{-13}	42.0%

4.3. Analysis of the Influence of LEO Enhancement Degree on Time Transfer Performance

To further investigate the influence of the enhancement level of LEO satellites on time transfer performance, experiments were designed with different numbers of LEO satellites. Four scenarios were considered for the LEO enhancement level, corresponding to 1, 2, 3, and 4 LEO satellites. Regarding the LEO satellite number control method involved in this paper, the selection strategy of three LEO satellites is taken as an example to illustrate the following: When the number of LEO satellites is more than 3, the first three satellites are retained according to the elevation angle. If a retained LEO satellite has an elevation angle lower than the cut-off elevation angle, the satellite with the higher elevation angle is selected for replacement.

Simultaneously, three time transfer links, namely pie1-ons1, harb-sydn, and ohi2-syog, were selected for conducting experiments on the LEO enhancement level. The diagrams depicting clock offsets for the pie1-ons1 link across the four scenarios are detailed in Figure 11, with the first-order differences shown in Figure 12. Similarly, the clock offset diagrams for the harb-sydn link under the four scenarios are shown in Figure 13, with the corresponding first-order difference results displayed in Figure 14. Lastly, the clock offset diagrams for the ohi2-syog link in the four scenarios are depicted in Figure 15, and the first-order difference results are exhibited in Figure 16.

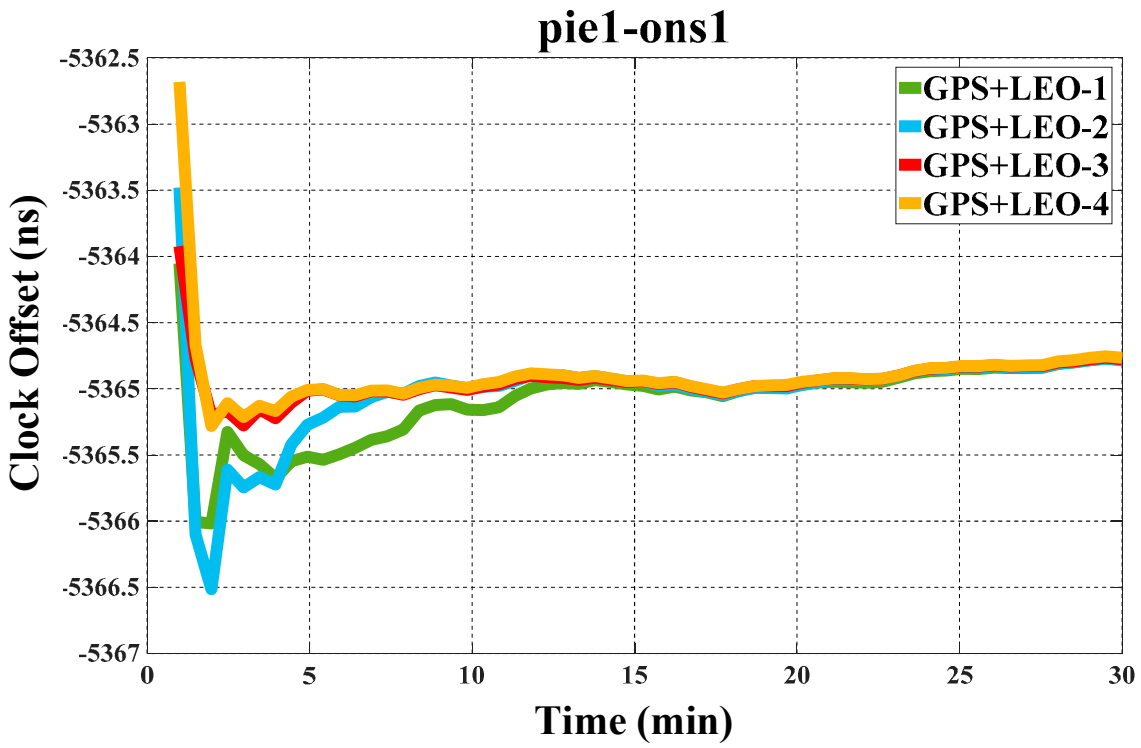

Figure 11. Clock offset diagram of pie1-ons1 time transfer link in the four enhancement scenarios.

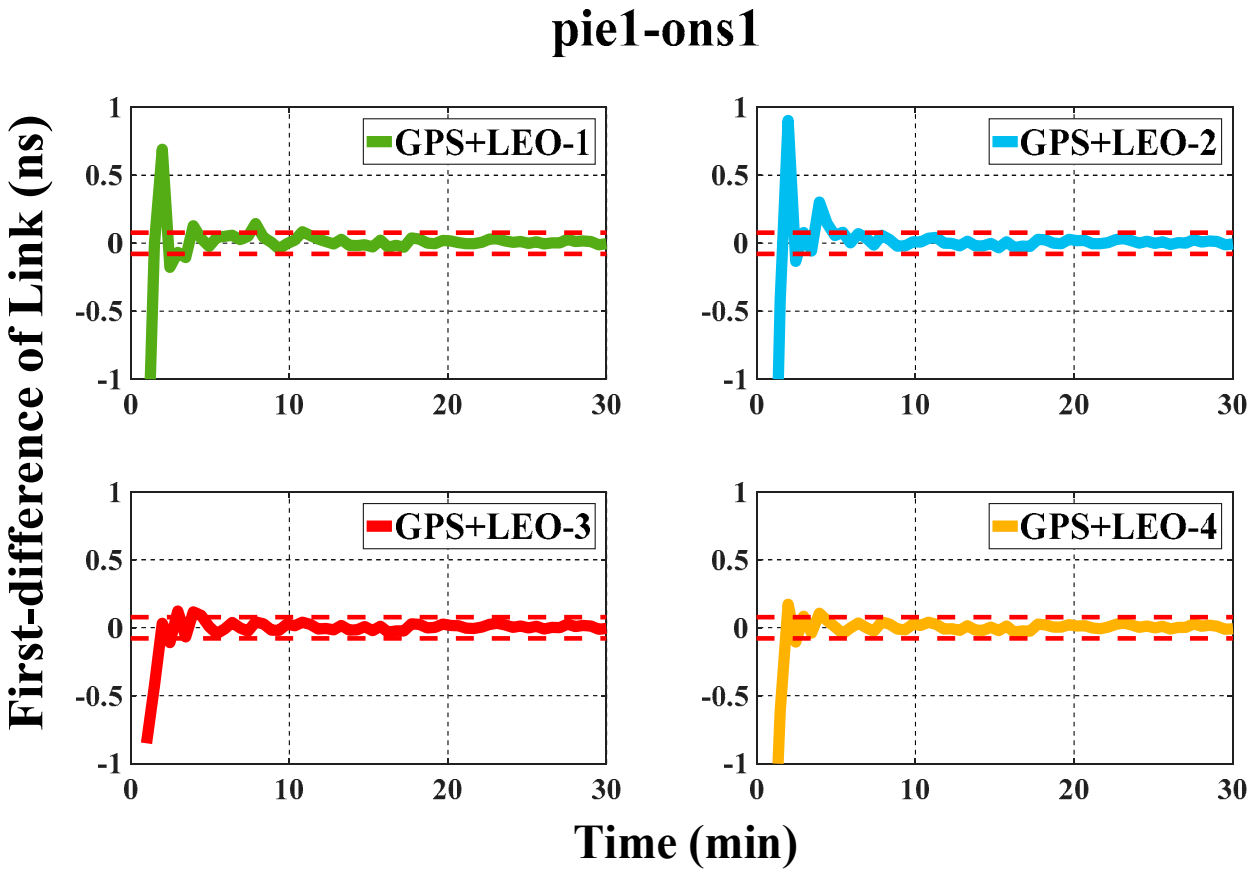

Figure 12. First-order difference diagram of pie1-ons1 time transfer link clock offset in the four enhancement scenarios.

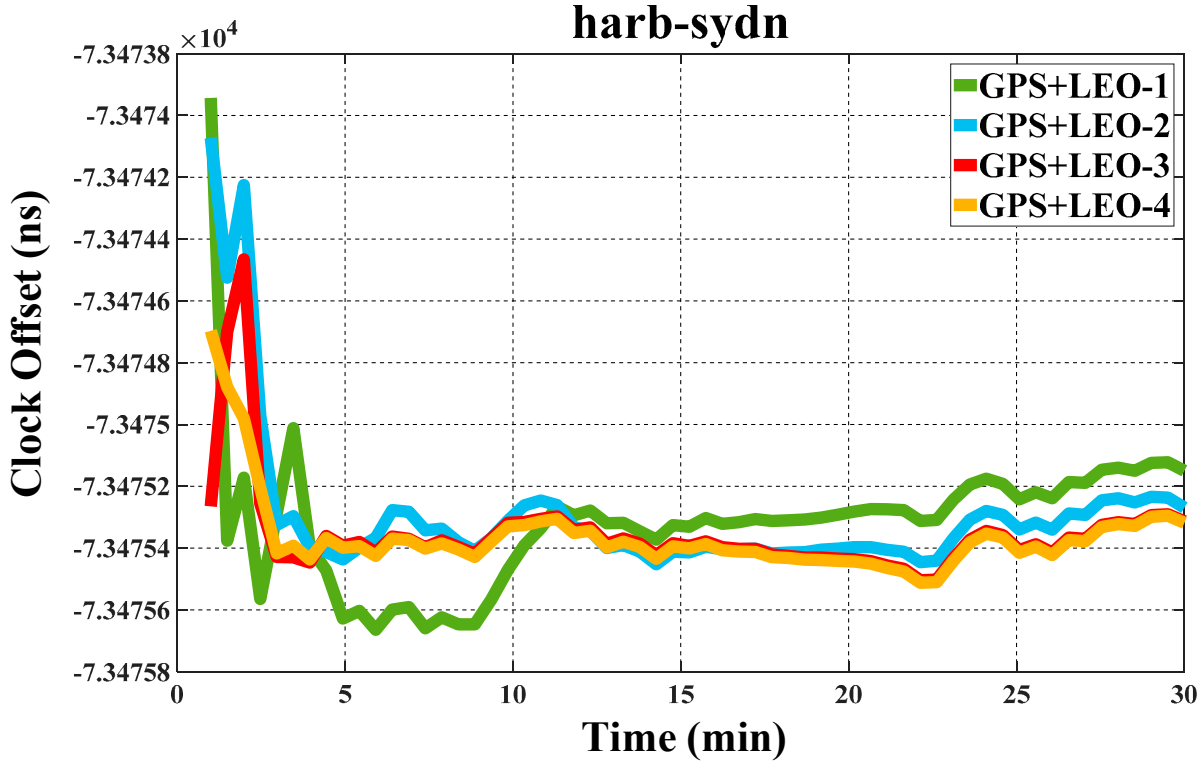

Figure 13. Clock offset diagram of harb-sydn time transfer link in the four enhancement scenarios.

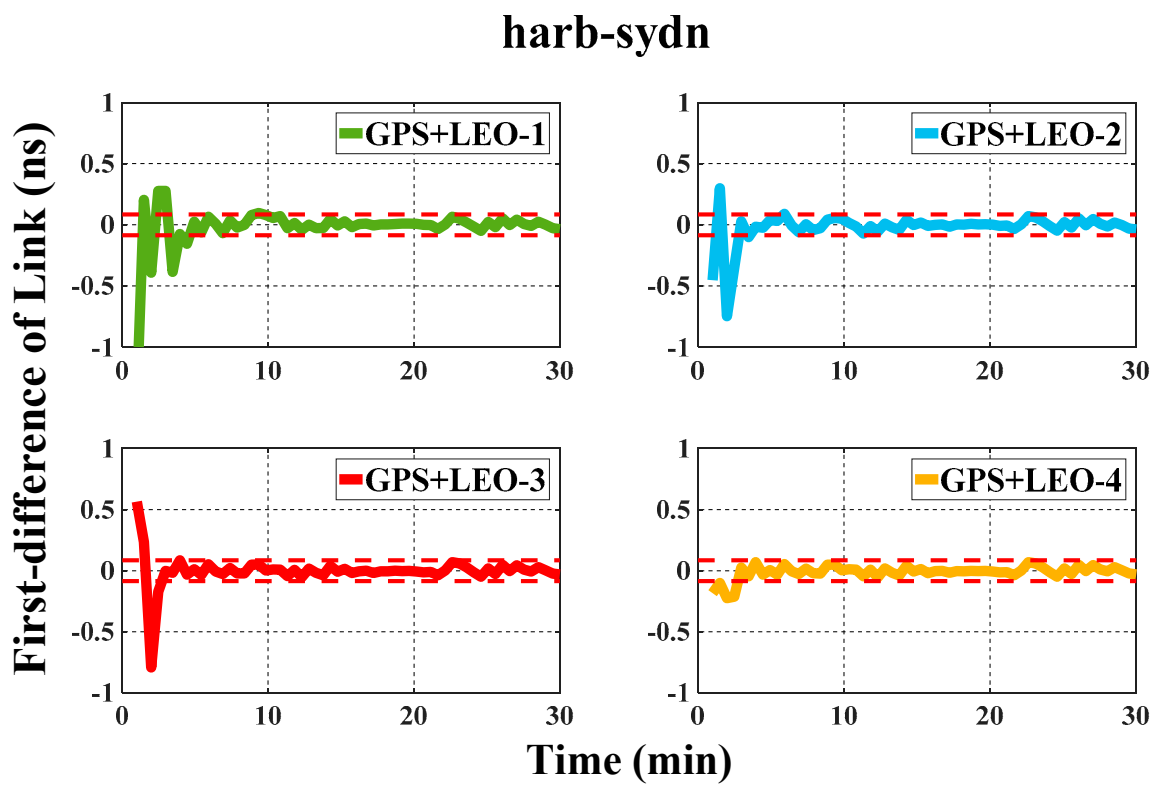

Figure 14. First-order difference diagram of harb-sydn time transfer link clock offset in the four enhancement scenarios.

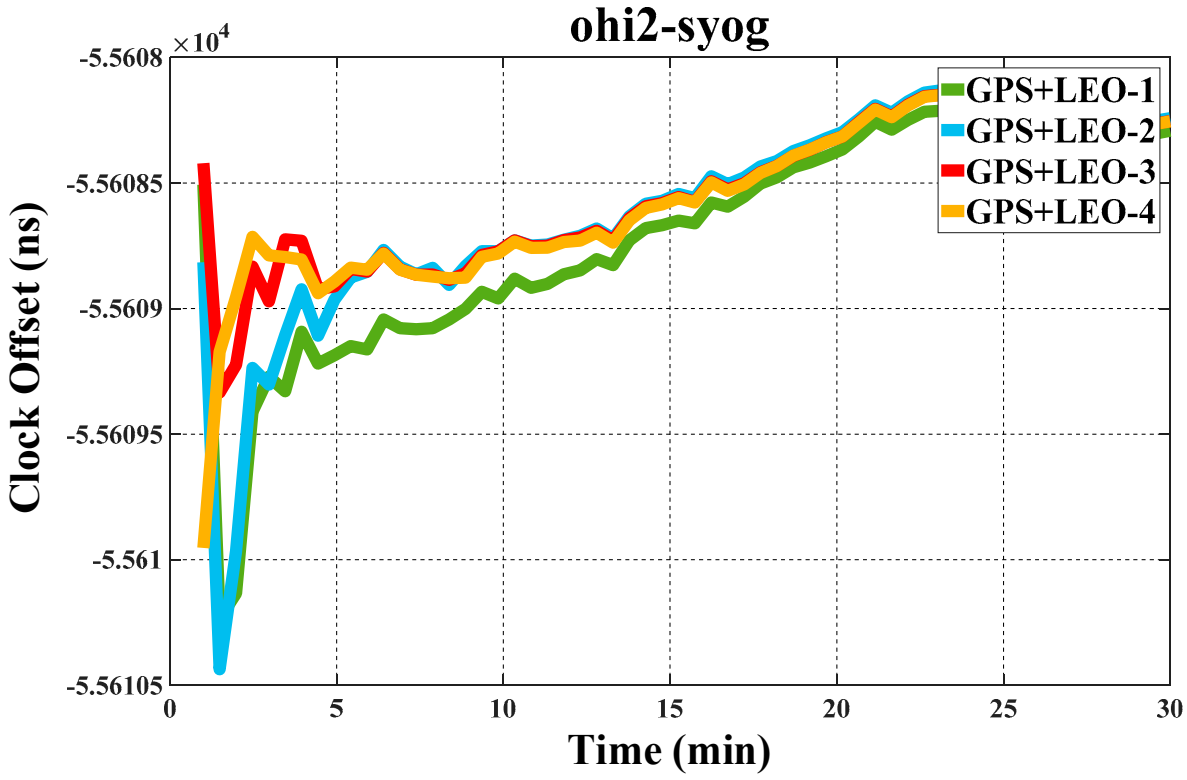

Figure 15. Clock offset diagram of ohi2-syog time transfer link in the four enhancement scenarios.

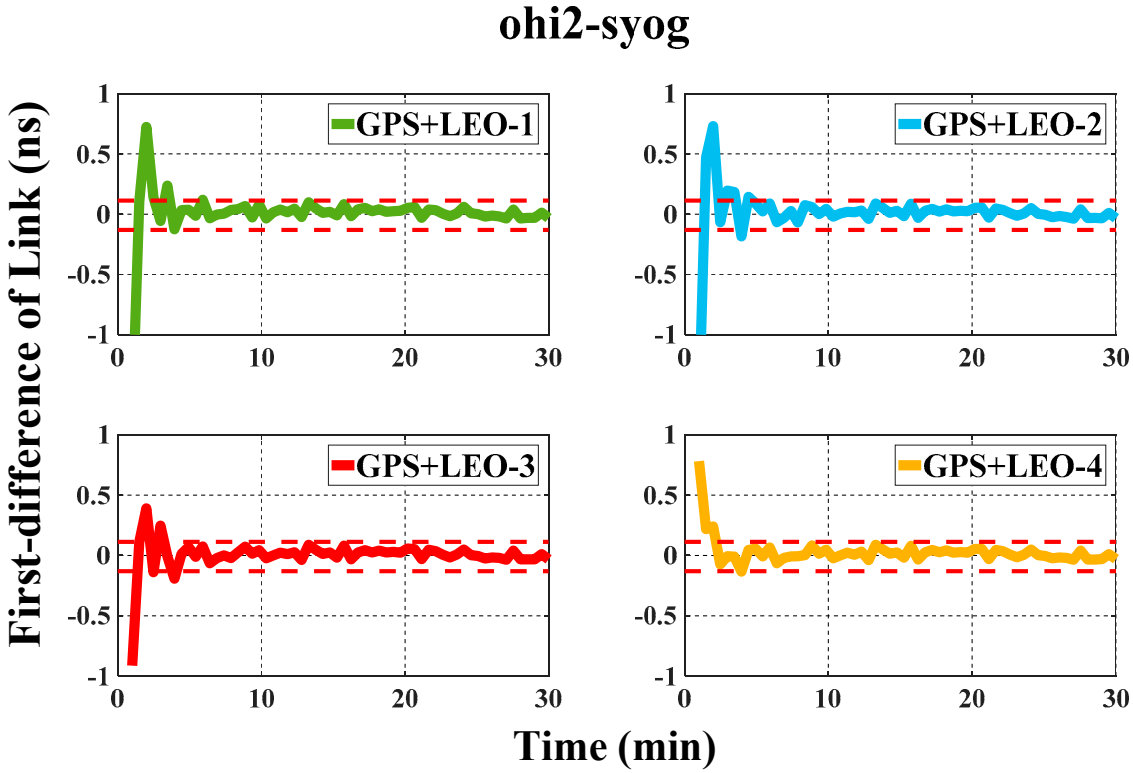

Figure 16. First-order difference diagram of ohi2-syog time transfer link clock offset in the four enhancement scenarios.

As the LEO satellite count increases, the effect of LEO enhancement was further strengthened, resulting in an enhanced convergence speed for the time transfer link. To examine the convergence speed, the convergence times of the three links in the four scenarios were tabulated, as shown in Table 8 and Figure 17. Under the four different LEO enhancement conditions, the trend in convergence of the three time transfer links was consistent, and convergence speed increased with satellite number. Combined with the data in Table 5, the convergence speed of the time transfer link clock offset under different LEO enhancement conditions was calculated and compared with that of the GPS. The results are summarized in Table 9. The largest improvement in convergence speed was observed in the harb-sydn link, which uses cesium as its clock frequency source. A sole LEO satellite increased convergence speed by 13.6%, whereas four satellites improved it by up to 77.3%. The ohi2-syog link with the mixed clock group showed little change in convergence speed according to the number of satellite. With one satellite, the convergence speed was almost the same as that of GPS. With three and four, the convergence speed increased by 33.3%. The aforementioned results further corroborate that LEO-augmented PPP has different degrees of applicability to time transfer links depending on the clock frequency source.

Table 8. Convergence time statistics of the three links across the four enhancement scenarios (min).

Number of Satellites	harb-sydn	ohi2-syog	pie1-ons1
1	9.5	6.0	11.0
2	6.0	4.5	5.5
3	4.0	4.0	4.5
4	2.5	4.0	4.0

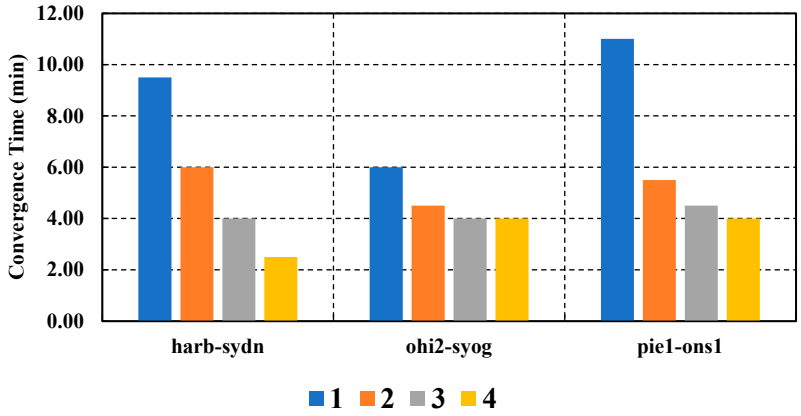

Figure 17. Convergence time histograms of the three links across the four enhancement scenarios.

Table 9. Convergence time percentage of improvement in the three links across the four enhancement scenarios.

Number of LEO	harb-sydn	ohi2-syog	pie1-ons1
1	13.6%	0.0%	4.4%
2	45.5%	25.0%	52.2%
3	63.6%	33.3%	60.9%
4	77.3%	33.3%	65.2%

Simultaneously, the standard deviation of the clock offset sequence of the time transfer link in the convergence interval is analyzed under the condition of different numbers of LEO satellites, and the results are shown in Table 10. The findings demonstrate that the stability of the time transfer link in the convergence interval increased with the number of satellites. Accordingly, with the increase in the number of LEO satellites, the combination of GPS + LEO has a better geometric shape, which is more conducive to improving the performance of PPP time transfer.

Table 10. Standard deviations of convergence interval clock offsets of the three links across the four enhancement scenarios (ns).

Number of LEO	harb-sydn	ohi2-syog	pie1-ons1
1	0.085	0.101	0.169
2	0.056	0.099	0.140
3	0.032	0.058	0.036
4	0.031	0.056	0.031

5. Conclusions

This study introduces a novel method for enhancing GNSS time transfer through the use of LEO satellites. The LEO satellite constellation was designed following a Walker constellation. The observational data from the LEO satellites were simulated based on data from all stations in the MGEX observation network. The GNSS observation data incorporated GPS data and precision products offered by the IGS. Utilizing these data, an enhanced PPP with LEO was developed. The receiver clock offset and time transfer link clock offset were additionally calculated. This study investigated the convergence performance and reliability of LEO-augmented GPS time transfer through experimental examples. Four scenarios were designed to assess the impact of LEO enhancement on time transfer reliability. Based on the comprehensive analysis and discussion presented above, the following conclusions were formulated:

(1) The receiver clock offset calculated using the LEO-augmented PPP model demonstrated accelerated convergence. The receiver clock offsets for three representative stations—areg, harb, and ons1—were examined. The convergence velocity of the receiver clock offsets was contrasted with those derived solely from GPS data. The convergence speed post-LEO augmentation was enhanced, with varying degrees of enhancement observed across different links. A convergence confidence interval was established to determine convergence time. The results showed that harb's cesium clock had the greatest increase in convergence speed at 65.0%. ons1's hydrogen clock had an increase of 50.0%, while areg's rubidium clock had the slowest increase at 18.8%. Therefore, LEO-augmented PPP affected clock offset convergence speeds differently on stations with different atomic clock frequency sources, reflecting the performance of the atomic clocks. The performance of atomic clocks directly determines the accuracy of time measurement, which in turn affects the measurement results of satellite signals and is indirectly reflected in the later data processing.

(2) The analysis focused on the convergence performance of the clock offsets of the ten time transfer links. The convergence speed of all the time transfer link clock offsets exhibited uniform performance. The convergence speed achieved with the LEO-augmented PPP was superior to that of the GPS-only model. PPP model based on LEO satellites fusion has different improvements in the convergence speed of time transfer links of different atomic clock types, and the improvement in the convergence speed of time transfer links of different baseline lengths is also different. There were no obvious differences in time transfer links at different latitudes. The enhanced convergence speed has been demonstrated to be more advantageous for securing the speed and real-time performance of GNSS time transfer.

(3) The standard deviation of the clock offsets for the time transfer link, as derived from both satellite constellation schemes during the convergence time range, was calculated. The PPP model based on LEO satellites fusion did significantly improve stability in the convergence interval. Additionally, the Allan deviation was employed to assess the frequency stability of the time transfer link clock offset in the convergence interval. The findings demonstrate that the frequency stability obtained by the PPP model based on LEO satellite fusion in the convergence interval was significantly better than that of the sole GPS. Consequently, the PPP model enriched with LEO satellite data positively influences the reliability of time transfer.

(4) Experiments involving varying quantities of LEO satellites demonstrated that an increase in LEO satellite data correspondingly improved the enhancement degree. This was mainly manifested as faster convergence speeds and higher stability in the convergence interval.

In summary, the time transfer method proposed in this study can effectively enhance the performance of time transfer. This will be beneficial for further advancing the development of time-frequency application services and industries, especially for mobile time synchronization terminals; it can improve their application efficiency and product performance.

Author Contributions: M.L. and R.T. provided the initial idea for this work and wrote this manuscript; M.L. designed the algorithm. Q.L., Q.C., J.C., P.Z. and X.L. contributed to the analyses of the results. All authors have read and agreed to the published version of the manuscript.

Funding: The work is partly supported by the National Key R&D Program of China and Shandong Province (grant No: 2021YFB3901300) and program of National Natural Science Foundation of China (grant No: 41974032, 42274019).

Data Availability Statement: The raw/processed data required to reproduce these findings cannot be shared at this time as the data also form part of an ongoing study.

Acknowledgments: This work was supported by the Chinese Academy of Sciences (CAS) programs of "High Level Talents".

Conflicts of Interest: The authors declare no conflicts of interest.

References

1. Zhang, P. The research of key technology and approach for time and frequency transfer based on GNSS carrier phase observation. *Acta Geod. Cartogr. Sin.* **2020**, *49*, 669.
2. Zhao, Q.; Pan, S.; Gao, C.; Gao, W.; Xia, Y. BDS/GPS/LEO triple-frequency uncombined precise point positioning and its performance in harsh environments. *Measurement* **2020**, *151*, 107216. [CrossRef]
3. Yang, X.; Li, X.; Hua, Y.; Jin, W.; Sun, B.; Li, W.; Qin, W.; Wu, M.; Wang, W.; Zhao, K. Technical Progress of Satellite Time Service and Time Transfer. *Navig. Position. Timing* **2021**, *8*, 1–10.
4. Liu, J.; Tu, R.; Zhang, R.; Huang, X.; Zhang, P.; Lu, X. A New Method of Real-Time Kinematic Positioning Suitable for Baselines of Different Lengths. *J. Navig.* **2021**, *74*, 143–155. [CrossRef]
5. Ge, M.; Gendt, G.; Rothacher, M.a.; Shi, C.; Liu, J. Resolution of GPS carrier-phase ambiguities in precise point positioning (PPP) with daily observations. *J. Geod.* **2008**, *82*, 389–399. [CrossRef]
6. Chen, X.; He, D.; Pei, L. BDS B1I multipath channel statistical model comparison between static and dynamic scenarios in dense urban canyon environment. *Satell. Navig.* **2020**, *1*, 1–16. [CrossRef]
7. Hsu, L.-T. Analysis and modeling GPS NLOS effect in highly urbanized area. *GPS Solut.* **2018**, *22*, 7. [CrossRef]
8. Zhao, C.; Sheng, C.; Zhang, B. Precise point positioning time transfer based on receiver clock offsets constraint. *GNSS World China* **2021**, *46*, 13–17.
9. Xu, Z.; Ding, X.; Wei, Z.; Xu, Y.; Han, P.; Zhuang, D. Based on BDS three frequency PPP precision time processing key technology and precision analysis. *Sci. Surv. Mapp.* **2020**, *45*, 23–27.
10. Lv, D.; Zeng, F.; Ouyang, X. Time Transfer Algorithm Using Multi-GNSS PPP with Ambiguity Resolution. *Acta Astron. Sin.* **2020**, *61*, 62–72.
11. Tu, R.; Hong, J.; Zhang, R.; Han, J.; Fan, L.; Zhang, P.; Liu, J.; Lu, X. GPS and BDS combined PPP model with inter-system differenced observations. *Adv. Space Res.* **2020**, *65*, 494–505. [CrossRef]
12. Enge, P.; Ferrell, B.; Bennett, J.; Whelan, D.; Gutt, G.; Lawrence, D. Orbital diversity for satellite navigation. In Proceedings of the 25th International Technical Meeting of The Satellite Division of the Institute of Navigation (ION GNSS 2012), Nashville, TN, USA, 17–21 September 2012; pp. 3834–3846.
13. Reid, T.G.; Neish, A.M.; Walter, T.F.; Enge, P.K. Leveraging commercial broadband leo constellations for navigating. In Proceedings of the 29th International Technical Meeting of the Satellite Division of the Institute of Navigation (Ion Gnss+ 2016), Portland, OR, USA, 12–16 September 2016; p. 2016.
14. Reid, T.G.; Walter, T.; Enge, P.K.; Sakai, T. Orbital representations for the next generation of satellite-based augmentation systems. *GPS Solut.* **2016**, *20*, 737–750. [CrossRef]
15. Ke, M.; Lv, J.; Chang, J.; Dai, W.; Tong, K.; Zhu, M. Integrating GPS and LEO to accelerate convergence time of precise point positioning. In Proceedings of the 2015 International Conference on Wireless Communications & Signal Processing (WCSP), Nanjing, China, 15–17 October 2015; pp. 1–5.
16. Ge, H.; Li, B.; Ge, M.; Zang, N.; Nie, L.; Shen, Y.; Schuh, H. Initial assessment of precise point positioning with LEO enhanced global navigation satellite systems (LeGNSS). *Remote Sens.* **2018**, *10*, 984. [CrossRef]
17. Su, M.; Su, X.; Zhao, Q.; Liu, J. BeiDou augmented navigation from low earth orbit satellites. *Sensors* **2019**, *19*, 198. [CrossRef] [PubMed]
18. Li, X.; Li, X.; Ma, F.; Yuan, Y.; Zhang, K.; Zhou, F.; Zhang, X. Improved PPP ambiguity resolution with the assistance of multiple LEO constellations and signals. *Remote Sens.* **2019**, *11*, 408. [CrossRef]
19. Li, B.; Ge, H.; Ge, M.; Nie, L.; Shen, Y.; Schuh, H. LEO enhanced Global Navigation Satellite System (LeGNSS) for real-time precise positioning services. *Adv. Space Res.* **2019**, *63*, 73–93. [CrossRef]
20. Ma, F.; Zhang, X.; Hu, J.; Li, P.; Pan, L.; Yu, S.; Zhang, Z. Frequency design of LEO-based navigation augmentation signals for dual-band ionospheric-free ambiguity resolution. *GPS Solut.* **2022**, *26*, 53. [CrossRef]
21. Hong, J.; Tu, R.; Zhang, P.; Zhang, R.; Han, J.; Fan, L.; Wang, S.; Lu, X. GNSS rapid precise point positioning enhanced by low Earth orbit satellites. *Satell. Navig.* **2023**, *4*, 11. [CrossRef]
22. Maurya, A.K.; Phanikumar, D.; Singh, R.; Venkatesham, K.; Singh, A.K. Effect of total lunar eclipse of 27th July 2018 on the D-region ionosphere by using VLF observations. *Adv. Space Res.* **2022**, *69*, 121–131. [CrossRef]
23. Böhm, J.; Niell, A.; Tregoning, P.; Schuh, H. Global Mapping Function (GMF): A new empirical mapping function based on numerical weather model data. *Geophys. Res. Lett.* **2006**, *33*, 25564. [CrossRef]